applied sciences

MDPI

Article

Dynamic Damping of Power Oscillations in High-Renewable-Penetration Grids with FFT-Enabled POD-P Controllers

Marta Bernal-Sancho [1,*], Marta Muñoz-Lázaro [1], María Paz Comech [2] and Pablo Ferrer-Fernández [1]

[1] Electrical Systems Department, CIRCE Technology Centre, 50018 Zaragoza, Spain; mmunoz@fcirce.es (M.M.-L.); pferrer@fcirce.es (P.F.-F.)
[2] Research Institute for Energy and Resource Efficiency of Aragón (Energaia), University of Zaragoza, Campus Río Ebro, Mariano Esquillor Gómez, 15, 50018 Zaragoza, Spain; mcomech@unizar.es
* Correspondence: mbernal@fcirce.es

Abstract: The growing integration of renewable energy sources, particularly photovoltaic (PV) and wind power, presents challenges such as reduced system inertia and increased susceptibility to inter-area oscillations. These issues, coupled with stricter regulatory demands for grid stability, highlight the urgent need for effective damping solutions. This study proposes a novel method for detecting and mitigating inter-area oscillations using a power oscillation damping (POD) controller enhanced by applying a Fast Fourier Transform (FFT). The controller's parameters are optimized through the Nobel Bat Algorithm (NBA) and fully implemented in DIgSILENT PowerFactory (DSPF). Simulations conducted on the New England IEEE-39 power system model under varying levels of renewable energy penetration demonstrate the model's capability to dynamically detect, mitigate, and deactivate oscillations once stability is achieved. This work addresses emerging regulations requiring oscillation damping systems and offers a framework for certifying POD controllers for real-world implementation, ensuring their adaptability to diverse energy systems and regulatory contexts.

Keywords: inter-area oscillation; power oscillation damping; photovoltaic plant; fast Fourier transform; Nobel bat algorithm; grid stability; DIgSILENT PowerFactory; power plant controller

Academic Editor: Yang Liu

Received: 15 January 2025
Revised: 30 January 2025
Accepted: 2 February 2025
Published: 4 February 2025

Citation: Bernal-Sancho, M.; Muñoz-Lázaro, M.; Comech, M.P.; Ferrer-Fernández, P. Dynamic Damping of Power Oscillations in High-Renewable-Penetration Grids with FFT-Enabled POD-P Controllers. *Appl. Sci.* **2025**, *15*, 1585. https://doi.org/10.3390/app15031585

1. Introduction

The exponential growth of renewable energy generation has significantly transformed the global power generation landscape. As the share of renewable power increases, particularly through wind farms (WFs) and photovoltaic (PV) plants, the inherent variability and lack of inertia associated with these sources pose new challenges for grid stability. These issues are especially evident in weakly interconnected networks, where disturbances can quickly propagate, amplifying oscillations and compromising system stability [1–3]. This increase in renewable energy sources heightens the vulnerability of power systems to low-frequency oscillations (LFOs), which can be classified into two main categories [4]: local and inter-area oscillations. While local oscillations, typically occurring between 1 and 2.5 Hz, are generally managed by Power System Stabilizers (PSSs) parametrized to damp them, inter-area oscillations occur at lower frequencies (typically between 0.1 and 1.0 Hz) and are particularly challenging. These oscillations involve large groups of generators oscillating against each other across weakly interconnected transmission lines, which increases the risk of system instability.

Notable incidents of inter-area oscillations, such as the 1996 Western System Coordinated Council (WSCC) blackout in the United States [5], the 2003 Northeast blackout [6], and the 2016 oscillatory event triggered by a line opening in the French–Spanish interconnection [7], underscore the urgent need for proactive measures to address grid stability challenges. These events, among others, highlight the severity of inter-area oscillations and the need for their early detection and mitigation. Effective damping strategies are increasingly necessary to ensure the stable operation of power systems with a high degree of renewable energy penetration. Several studies have already focused on stability due to the growing concern about low-frequency oscillations in different countries, focusing on the problem of inter-area oscillations. For example, the impact of resonance on inter-area oscillations in the Nordic power system [8,9], the analysis of inter-area oscillations in the UCTE/CENTREL power system [10,11], or the improvement of the damping of the inter-area oscillatory mode between Scotland and England [12].

Growing concern has also highlighted the need for effective grid stability measures at the regulatory level, particularly regarding the implementation of power oscillation damping (POD) controllers. At the European level, Commission Regulation (EU) 2016/631 [13] specifies that renewable generators must be capable of damping oscillations when required by the system operator, ensuring grid stability in critical situations. ACER Recommendation 03-2023 Annex 1 [14] provides further guidance on implementing POD functionalities in high-renewable systems, emphasizing the need for generators to mitigate low-frequency oscillations. In Spain, the draft Operation Procedure (PO) 12.2 [15] requires renewable plants, especially type D (plants whose connection point voltage is equal to or greater than 110 kV or whose maximum power exceeds 50 MW), to have a POD controller capable of damping inter-area oscillations in the range of 0.1 Hz to 1.0 Hz, ensuring integration into the national grid. Additionally, the importance of POD controllers is reinforced by the POD Controller Implementation Guide [16], which outlines the steps and requirements for their implementation, highlighting their critical role in stabilizing the grid and supporting higher renewable energy penetration.

Many studies have focused on the installation of POD controllers within Flexible AC Transmission Systems (FACTS) [17–19], as well as in PV plants [20,21] and WFs [22–25], testing their efficiency in isolated and controlled simulations. Some investigations have also incorporated measurements from Phasor Measurement Units (PMUs), enabling the monitoring of inter-area oscillations [26] and real-time data integration to assess the performance of POD controllers in existing power systems [27–29]. Despite this, these works are often limited by short-duration simulations or the manual activation of POD controllers, which restricts the system's ability to respond autonomously to grid fluctuations. Furthermore, while activation functions have been employed to detect oscillations in some research, such as the Fast Fourier Transform (FFT) [30–32], the Prony Analysis [33–35], and the Matrix Pencil Method, among others [36,37], these studies have not fully addressed the complexities of grid modeling or the need for effective POD controller parametrization under varying grid conditions.

Moreover, extensive research explores the coordination of damping controllers between PSSs and POD using different optimization algorithms, such as Particle Swarm Optimization (PSO) [38,39] and the Nobel Bat Algorithm (NBA) [40,41], among others [42,43]. However, they often neglect the critical aspect that is POD activation. While these studies provide valuable insights into the optimal configuration of POD controllers, they typically overlook the real-time, dynamic activation of these controllers. This aspect is critical for managing renewable energy integration challenges in modern power grids.

The main objective of this article is to develop a comprehensive approach to oscillation detection, POD activation, inter-area oscillation damping, and POD deactivation, carrying

out the entire process within DIgSILENT PowerFactory (DSPF) [44] without interruptions. This approach simulates complete POD operation in a real-world environment and represents a novel contribution, as no previous works have examined the entire process in a single simulation environment without requiring external software or stopping the simulation. This study focuses on the entire process, detailing the detection technique (FFT is used, noted for its computational efficiency [45]), the POD-P controller (more versatile than POD-Q when considering frequency inputs and multiple oscillations [46]), and the POD tuning method (using NBA, demonstrated to outperform PSO even with fewer iterations [47]).

The New England IEEE-39 power system model is extended with PV plants for realistic simulation. The Power Plant Controller (PPC) is modified to incorporate a POD-P controller and detection functions, creating a realistic scenario with three renewable generation conditions, reflecting real-world variability. This study establishes a comprehensive foundation for future work in integrated grid stability simulations. Examining realistic conditions with varying availabilities of renewable energy highlights critical aspects of stability control in grids with high renewable penetration, providing valuable insights for future deployments of POD controllers in renewable-dominant systems.

2. Definition of POD Controller

The main objective of the POD is to damp power oscillations. A POD controller, when implemented in FACTS devices, WFs, or PV plants, provides damping capabilities similar to those of synchronous generators with PSSs. The POD controller can be installed in the PPC to send a unified damping signal to all generators or each generator individually. In this article, the POD controller is configured within the PPC of the PV plants.

The POD-P controller operates as a supplementary control loop, adding an extra reference signal (dP_POD) to the PPC active power control, as shown in Figure 1.

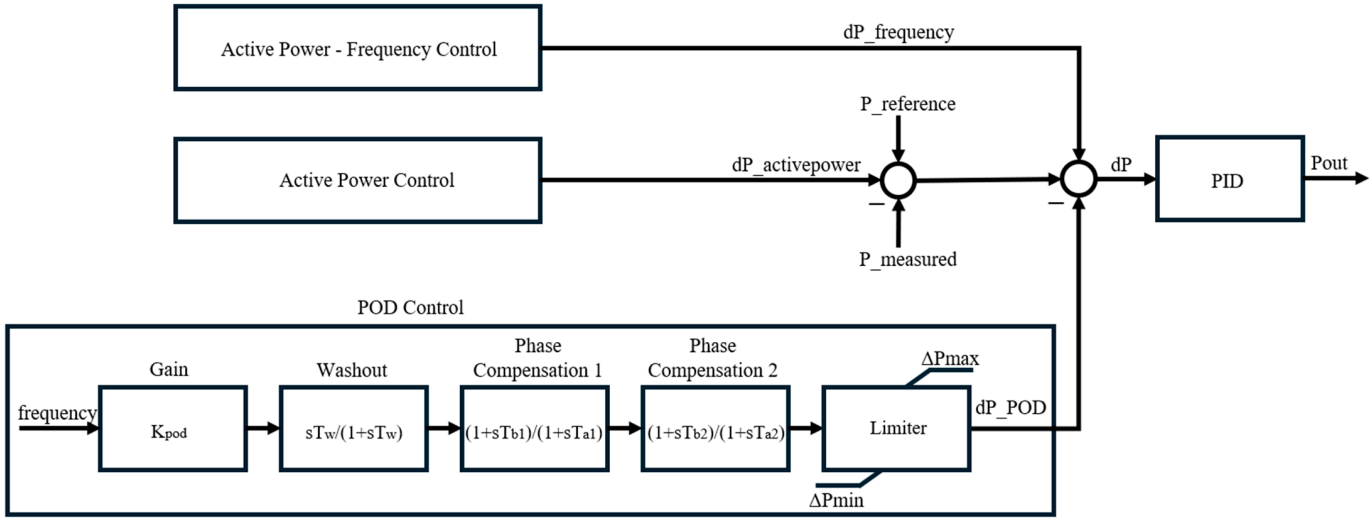

Figure 1. POD-P controller block diagram.

As mentioned in Section 1, this article considers only the active-power POD-P, as it has been shown to be more versatile than POD-Q for damping multiple oscillations [46].

The POD controller consists of three main parts [16]: a stabilizer gain Kpod, a washout filter with the time constant Tw, and two-phase compensation blocks with the time constants Tb1, Ta1, Tb2, and Ta2. Moreover, a limiter is applied to the output. The POD processes oscillation signals from the power system, such as active power, voltage, or frequency. This study uses the frequency at the PV plant terminal as the input signal. The output of the

POD-P controller (dP_POD) provides the command to damp oscillations by modifying the generator controller's original active power signal [16].

3. Optimization of the POD-P Parameters by NBA

To ensure the optimal performance of the POD-P controller, accurate tuning of the parameters (KPOD, Tw, Tb1, Ta1, Tb2, and Ta2) is crucial. Proper tuning directly impacts the system's ability to effectively damp oscillations and maintain stability in the presence of fluctuating renewable generation. This article employs the NBA to optimize these parameters, enhancing the damping ratio of the electromechanical mode. By improving the damping ratio, the system's stability is reinforced, ensuring robust performance under perturbances. The NBA is chosen due to its proven efficiency and superior convergence properties, as demonstrated in [47]. This includes its ability to handle complex, multi-modal objective functions and success in tuning controllers within high-renewable-penetration systems. Specifically, it has been shown to outperform traditional optimization methods, such as PSO, by achieving faster convergence and better computational efficiency under similar scenarios. Its robustness, particularly in systems with varying dynamic conditions, such as those in PV plants integrated into modern grids, makes it a reliable choice [47].

The NBA, an enhanced version of the original Bat Algorithm (BA) developed by Yang in 2010 [48], is inspired by the echolocation behavior of bats. In this algorithm, bats navigate by emitting sound waves and analyzing returning echoes, a process simulated to explore and exploit the solution space effectively. Introduced by Meng in 2015 [49], the NBA incorporates adaptive Doppler compensation, stochastic habitat selection, and inertia weight adjustments to improve search efficiency. This algorithm is particularly effective for dynamic systems characterized by high renewable penetration.

In the NBA, each bat represents a candidate solution characterized by a position, velocity, and frequency, which are updated iteratively to improve the objective function. For the POD controller, the system's damping ratio is chosen as the objective function [50]. The limit used in this objective function has been selected according to Spanish operating procedures [51], which establish a damping ratio threshold of 5% to define acceptable system stability, with higher damping ratios indicating greater stability. The mathematical formulation of the algorithm is thoroughly explained in [47] and [49].

The POD-P parameters, KPOD, Tw, Tb1, Ta1, Tb2, and Ta2, are constrained within a range based on the operational limits specified in [16]. The NBA iteratively refines these parameters, balancing exploration (searching the solution space) and exploitation (refining promising solutions). This study runs the NBA with 30 bats and 50 iterations. As a result, the POD-P controller achieves an optimal configuration, producing a corrective signal, dP_POD, that dynamically adjusts the PPC's active power setpoint, effectively damping oscillations and maintaining stability. The optimized parameters for each POD-P controller are determined using a base scenario and remain fixed throughout all subsequent simulations conducted in this research.

4. Definition and Implementation of Fast Fourier Transform

The FFT algorithm is widely used to analyze the frequency content of power system signals and detect the presence of power oscillations and their frequencies, including their oscillatory modes [31,32]. While FFT may be less accurate than other oscillation detection methods, such as the Matrix Pencil Method or Prony Analysis, it offers advantages in terms of computational efficiency, as detailed in [45]. This efficiency, coupled with its simpler implementation, makes FFT suitable for inter-area oscillation detection, where computational efficiency is prioritized over the results. The FFT transforms a signal in the time domain into its representation in the frequency domain, providing information about

the frequencies and amplitudes of this signal. This facilitates the analysis of the frequency components within the signal. Applying the FFT to the measured signal in inter-area oscillation detection allows the oscillation frequencies of interest (between 0.1 and 1 Hz [4]) to be analyzed and identified within a moving window, which is continuously updated as the simulation runs.

The FFT is introduced in DSPF as a function programmed in C, encapsulated in a .dll file. The output of the block is the trigger signal for the POD-P controller, Enable_POD. The FFT value in the area of interest (0.1–1 Hz) must exceed a threshold to trigger this signal. This threshold is set at 15 mHz, the trigger frequency specified in the POD Controllers Implementation Guide [16].

Exceeding this FFT threshold signifies the presence of power oscillations within the specified frequency range, subsequently activating the POD-P controller. The FFT calculation uses 10,000 samples with a time step of 0.5 ms, ensuring a detailed frequency analysis. Additionally, the calculation is performed continuously throughout the simulation. During the RMS simulation, the FFT operates over a floating window of 5 s, with recalculations occurring every 0.5 s. The FFT value obtained in the current window is compared with the value from the previous window to determine whether to activate or deactivate the POD-P, providing a double confirmation mechanism to enhance reliability. The POD-P controller activates or deactivates only when the FFT results from two consecutive time windows yield the same result (both 1 for activation or both 0 for deactivation). A 5 s delay is also implemented before deactivation to better replicate real-world operational procedures.

This approach improves upon previous FFT-based POD solutions by integrating a robust activation and deactivation mechanism that minimizes false positives through double confirmation and a time delay. Furthermore, the function is encapsulated in a .dll file within DSPF, enabling inter-area oscillation detection during simulation runs entirely within the software environment. These enhancements ensure reliable activation through real-time simulation with varying network conditions, providing a balance between computational efficiency and robust oscillation damping.

5. Detection and Damping Methodology

The proposed methodology summarized in Figure 2 allows us to detect inter-area oscillations, dynamically activate POD-P controllers, and deactivate them once oscillations are mitigated, all within the DSPF environment. The control logic relies on two key variables derived from the FFT output: Enable_POD and Internal_variable.

To continuously monitor system signals, our methodology employs an FFT algorithm that detects frequencies within the inter-area oscillation range (0.1–1 Hz). The FFT operates within a floating window of 5 s, recalculating every 0.5 s.

Under normal operating conditions, Internal_variable and Enable_POD are zero. If the oscillatory magnitudes calculated by the FFT exceed the predefined threshold of 15 mHz, meaning that an inter-area oscillation has occurred, the Internal_Variable changes to 1. The FFT output is updated every 0.5 s, and a new value of Internal_Variable is set and compared to its previous value to verify consistency and minimize false positives. Activation occurs (Enable_POD = 1) instantaneously when the FFT calculated for two consecutive cycles equals one (Internal_Variable = 1).

A counter is implemented to manage the deactivation of the POD-P controller (Enable_POD = 0). Deactivation occurs when the FFT value remains at zero for two consecutive cycles (Internal_variable = 0). Additionally, if no change is detected in Internal_variable for 5 s (Counter = 10), the Enable_POD variable transitions to a deactivated state, ensuring that the system has fully stabilized before disabling the controller.

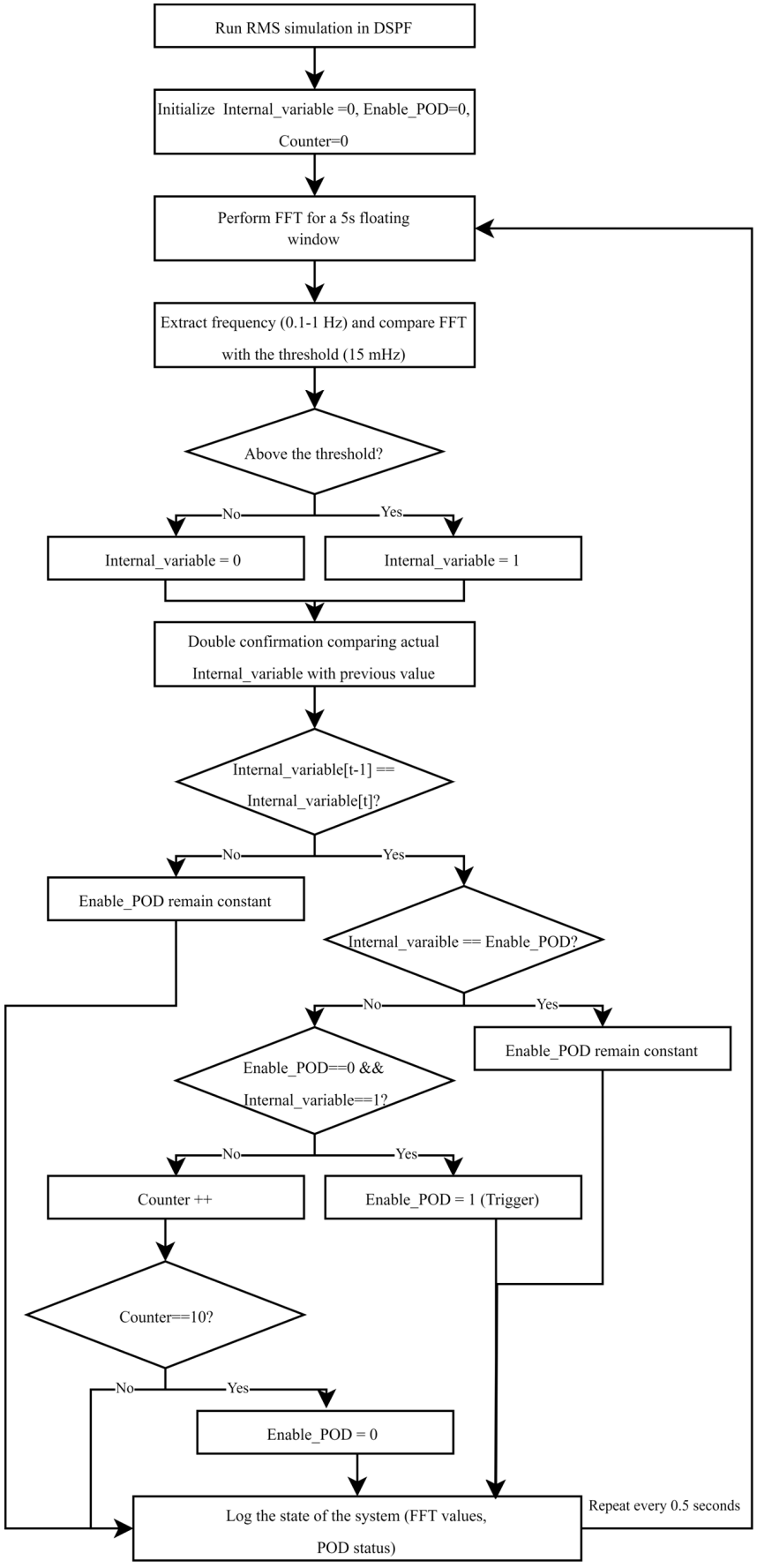

Figure 2. Methodology flowchart.

Upon activation, the POD-P controller generates a corrective signal, dP_POD (see Figure 1, Section 2), which dynamically adjusts the active power setpoint of the PPC. This modification allows the PV plants to contribute to damping the detected oscillations by modifying their active power output. As a result, the oscillatory behavior of the system is effectively mitigated, restoring system stability.

6. Network Description

The methodology presented in Section 5 has been simulated in a test network based on the New England IEEE-39 model, which provides a simplified representation of the northeastern U.S. transmission system [52]. The original IEEE-39 model consists of 39 buses, 10 generators, 19 loads, 34 transmission lines, and 12 transformers. Figure 3 presents a single-line diagram of the network. The different colors correspond to the different voltage levels: 345 kV (light blue), 230 kV (dark red), 16.5 kV (red) and 0.69 kV (blue).

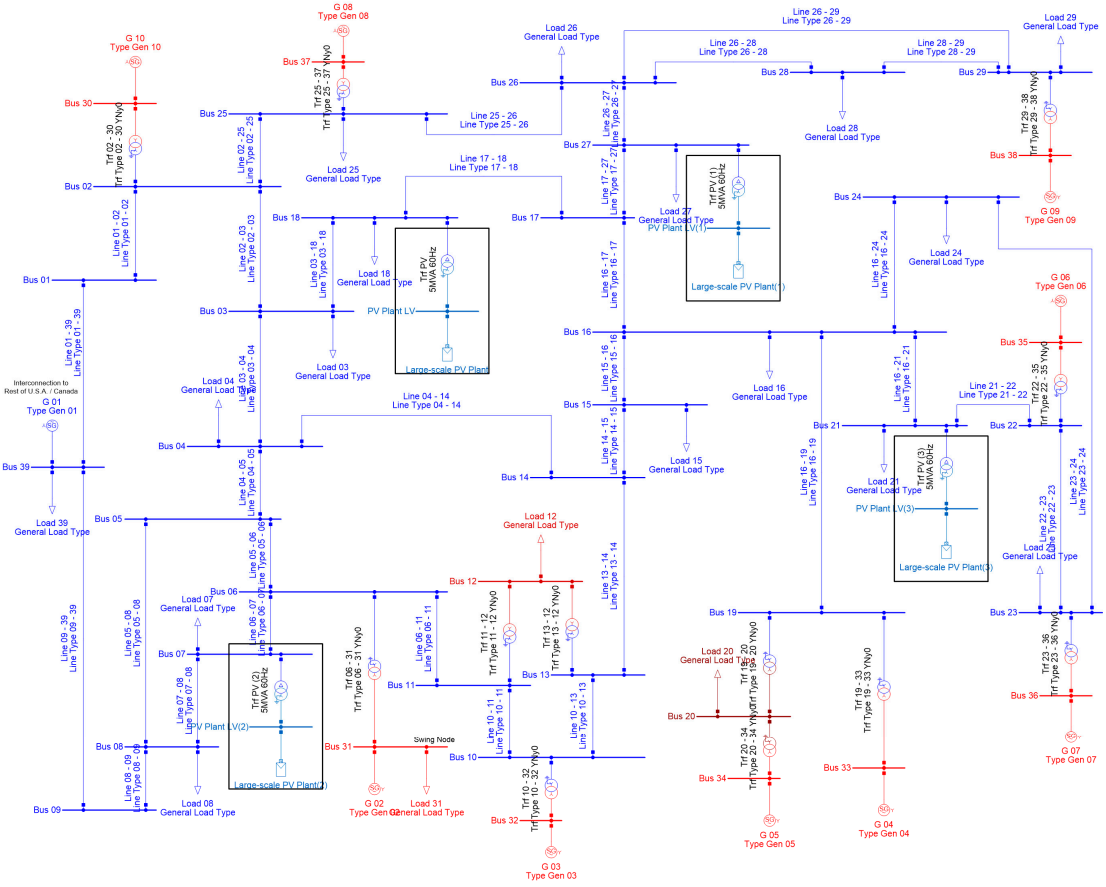

Figure 3. Modified New England IEEE-39 power system model.

In this model, Generator G01 represents the interconnection with the external transmission system, while Generator G02 is the slack bus. Active power dispatch and controlled terminal voltage magnitudes are assigned to the remaining generators. The technical specifications for all grid components, including generators, loads, transmission lines, and transformers, are available in [53].

The synchronous generator controllers include Automatic Voltage Regulators (AVRs), modeled as IEEE Type 1 rotating excitation systems in accordance with [54]. The governor models vary: IEEE Type G1 (steam turbine) is applied to Generators G02–G09, and IEEE Type G3 (hydro turbine) is used for Generator G10. To isolate and evaluate the performance of the POD-P controller, Power System Stabilizers (PSSs) are disabled throughout the study.

To assess scenarios with high levels of renewable energy penetration, this study integrates four PV plants into the system to analyze their impact on power oscillation damping. Figure 3 highlights these PV plants (marked with black squares), which are distributed across the grid to avoid localized effects and ensure a realistic simulation of renewable integration. Details regarding the rated power of the PV plants and the active power setpoints across scenarios are provided in Section 6. The PV controllers and generators are modeled using the WECC WT Type 4A model from the DSPF library [44]. These PV plants are equipped with PPCs that incorporate POD-P controllers designed to modulate active power and damp oscillations, as detailed in Section 2. The POD-P controller parameters are optimized using the NBA, as explained in Section 3, and remain fixed throughout the simulations.

7. Definition of the Simulation Scenarios

The simulation scenarios ensure a realistic approximation of future renewable energy production and its variability. This approach aligns with the PNIEC target of achieving 81% renewable generation by 2030 [55]. To facilitate this, the installed nominal PV power is set at 80% of the total synchronous generation capacity in the initial scenario, simulating various penetration levels. Consequently, the total nominal power of the four PV plants is equal to 80% of the total generation capacity of the grid. Initially, synchronous generators produce 6140.8 MW without the PV generators connected. Based on this, the nominal power of each PV plant is set at 1228.16 MW.

The scenarios range from 80% to 20% renewable generation, aligning with the expected future conditions of the grid. The 80% renewable generation scenario is based on the targets established by the PNIEC [55], while the 20% represents a low-renewable-penetration scenario, as renewable generation on the grid is unlikely to be zero. The scenarios are structured as follows:

- Scenario 1: PV plants generate 20% of the total grid power, with synchronous generators contributing 80%.
- Scenario 2: grid power is equally shared between PV plants and synchronous generators, each supplying 50%.
- Scenario 3: 80% of the grid generation is supplied by PV plants, while synchronous generators contribute 20%, consistent with the PNIEC target.

Operational constraints are explicitly considered, particularly in scenarios where PV plants operate at their maximum rated capacity. Under these conditions, the saturation of the active power output can restrict the POD-P controller's ability to effectively mitigate oscillatory events due to its limited capacity for further active power adjustments. This limitation is especially critical in Scenario 3, where PV plants operate at 100% of their nominal capacity, pushing the system to its operational limits. To overcome this challenge, an anti-windup filter is integrated into the PID controller. This filter dynamically limits the controller's response during saturation, preventing excessive integral windup and ensuring stable system performance under extreme conditions. Consequently, in Scenario 3, simulations are conducted with and without the anti-windup filter to evaluate its impact on the POD-P controller's effectiveness when the PV plants operate at full capacity.

Table 1 summarizes the three generation scenarios considered. The variation in the total power generated arises from the grid reference machine, which does not have a predefined active power setpoint but produces the amount needed for the grid to converge and operate correctly.

Table 1. Simulated scenarios.

Scenario	PV Active Power		Synchronus Machine Active Power		Total Generation [MW]
	P_PV [p.u.]	P_PV [MW]	P_synch [p.u.]	P_synch [MW]	
1	0.2	1228.16	0.8	4896.4	6158.54
2	0.5	3070.4	0.5	3057.5	6127.9
3	0.8	4912.64	0.2	1245.9	6124.56

8. Simulation Results

This section analyzes the results of the three scenarios presented in Section 7, focusing on the system's ability to mitigate inter-area oscillations under varying levels of renewable penetration and its response to consecutive events. For all scenarios, two events are considered (see Figure 3):

- A short-circuit at terminal 16 with a duration of 0.06 s.
- A short-circuit on line 03-04, followed by a switching event 0.25 s later.

These events are simulated in a continuous-time domain, where the FFT function individually detects the oscillations in each of the four PV plants by analyzing the frequency at their connection terminals, triggering and deactivating the POD-P controller as required to damp inter-area oscillations effectively.

The grid's electromechanical mode corresponds to an inter-area oscillation at 0.65 Hz, representing the system's natural oscillatory frequency. In the initial scenario, without PV generation, the electromechanical mode exhibits a damping ratio of 8.89%, which is above the stability threshold of 5% [51]. Variations in generation across scenarios significantly impact the stability of this mode, displacing it toward more unstable regions as renewable penetration increases and system inertia decreases. In all scenarios, both events generate inter-area oscillations, with Generator G01 oscillating against the rest of the system at 0.65 Hz.

The simulations replicate real-world conditions with varying levels of renewable penetration and consecutive events, validating the POD-P controller's autonomous activation and its reliability in damping oscillations. The simulations are performed in the time domain (RMS). Additionally, eigenvalue analyses are conducted to determine the damping ratio of the electromechanical mode for each scenario. These analyses provide a complementary and quantitative measure of system stability, enhancing the robustness of this study's findings.

8.1. Scenario 1

In Scenario 1, PV plants account for 20% of the total generation of the grid, while synchronous generators provide 80%. The PV plants contribute 1228.16 MW, while synchronous generation produces 4896.4 MW (see Table 1).

Initially, the simulation is executed with the FFT detection function disabled to observe the system's natural oscillatory response without POD-P controllers. The aggregation of PV plants reduces the damping ratio of the electromechanical mode to 3.19%, below the 5% stability threshold [51], increasing the system's susceptibility to disturbances. Figure 4a displays the frequency of all grid terminals. The oscillations observed at 5 s and 80 s correspond to the terminal and the line short-circuit (followed by its switching) events, respectively. As the system is initially unstable, these disturbances lead to inter-area oscillations that propagate over time. Figure 4b focuses on the frequency of the PV plant terminals and the synchronous generator speeds.

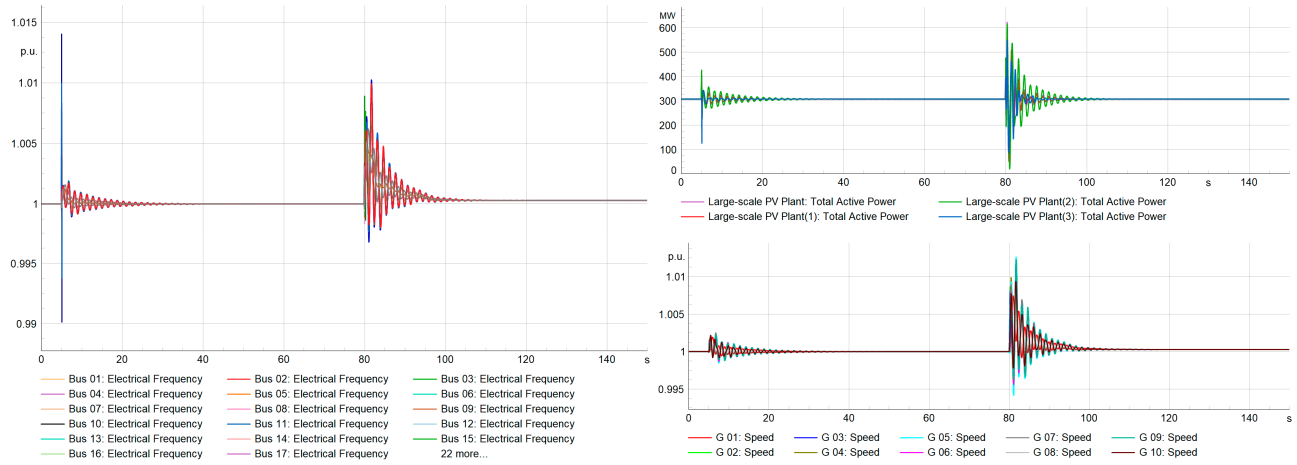

(**a**) (**b**)

Figure 4. Scenario 1. System response without the POD-P controller activated following the terminal short-circuit event (t = 5 s) and the line short-circuit event (t = 80 s): (**a**) frequency at all grid terminals [p.u.]; (**b**) frequency at PV terminals [p.u.] and speed of synchronous generators [p.u.].

When the FFT detection function is enabled, the system identifies and damps oscillations via the POD-P controller, which modulates the PPC active power setpoint. The activation of the POD-P controller, with appropriately tuned parameters, increases the damping ratio of the electromechanical mode to 11.86%, exceeding the stability threshold of 5%. Consequently, the system exhibits enhanced stability under disturbances, effectively mitigating oscillations. Figure 5a highlights the frequency response across all terminals with the POD-P controller activated, demonstrating the effective damping of inter-area oscillations. Figure 5b provides a focused view of the frequency at the PV plant terminals and the synchronous generator speeds, confirming that the system achieves stability.

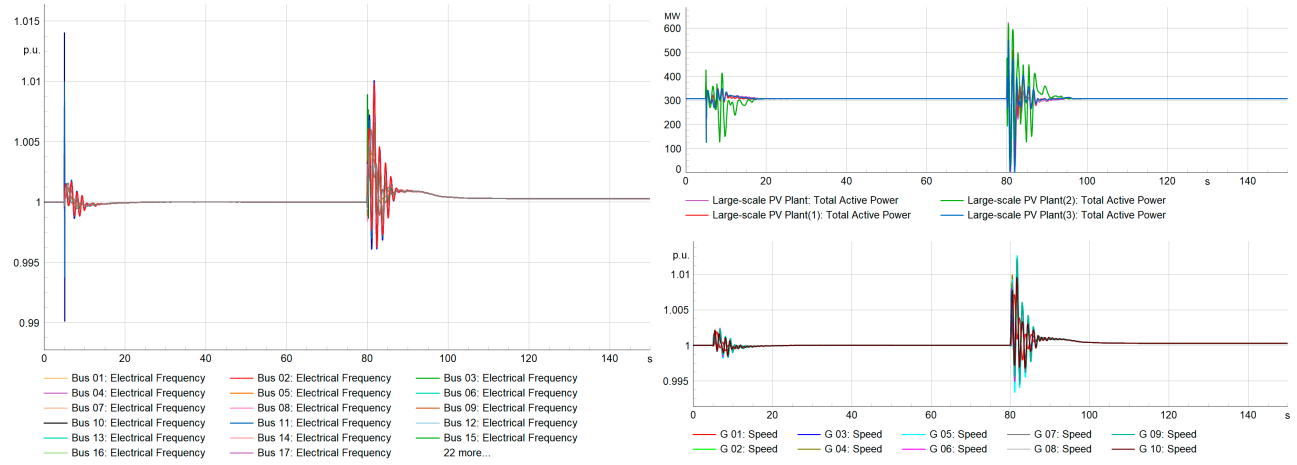

(**a**) (**b**)

Figure 5. Scenario 1. System response with the POD-P controller activated following the terminal short-circuit event (t = 5 s) and the line short-circuit event (t = 80 s): (**a**) frequency at all grid terminals [p.u.]; (**b**) frequency at PV terminals [p.u.] and speed of synchronous generators [p.u.].

For clarity, Figure 6 shows the FFT-triggered activation signal Enable_POD of the POD-P controllers and the corresponding adjustments to the PPC active power setpoint Pout for each controller. Upon activation, the POD-P controllers dynamically modify the active power setpoint to mitigate oscillatory behavior. Once the inter-area oscillations are

sufficiently dampened, the POD-P controllers deactivate, restoring the PPC active power setpoints to their pre-disturbance values. The same process is repeated for the second event.

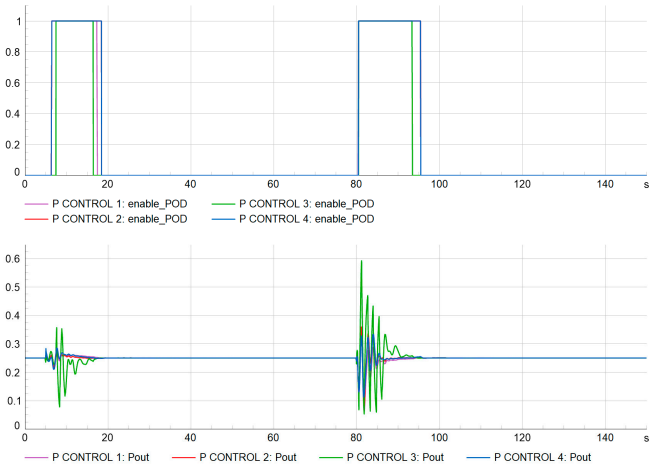

Figure 6. Scenario 1. POD-P activation signal *Enable_POD* and PPC active power setpoint *Pout* for each PV plant [p.u.].

8.2. Scenario 2

In Scenario 2, PV plants supply 50% of the total generation of the grid, with synchronous generators contributing 50%. This corresponds to 3070.40 MW from the PV plants and approximately 3057.5 MW from synchronous generation (see Table 1).

The system is first simulated with the FFT detection function disabled to observe the impact of increased renewable penetration. The integration of PV plants reduces the damping ratio of the electromechanical mode to 1.76%, reflecting the reduced stability of the system as renewable penetration increases. Figure 7a shows the frequency response of the grid terminals. Compared to Figure 4a, the initial peak is narrower, but the oscillations persist for a longer duration. This behavior is attributed to the diminished system inertia, which limits the system's ability to resist immediate changes in frequency following a disturbance, resulting in a smaller initial frequency deviation. However, the lower damping ratio exacerbates the system's susceptibility to sustained oscillations, leading to their prolonged decay. Figure 7b focuses on the frequency at the PV plant terminals and the synchronous generator speeds, highlighting the longer-lasting oscillatory behavior.

Once the FFT detection function is enabled, the POD-P controller actively damps the oscillation by adjusting the active power setpoint in the PPC. With the POD-P controller activated, the damping ratio increases to 10.61%, demonstrating the effectiveness of the control mechanism in stabilizing the system despite the reduced inertia. Figure 8a illustrates the significant reduction in frequency oscillations across all grid terminals, showcasing the damping mechanism's effectiveness. Figure 8b zooms in on the frequency at the PV plant terminals and synchronous generator speeds, highlighting the stabilized response.

Figure 9 illustrates the FFT-triggered activation signal Enable_POD of the POD-P controllers, along with the corresponding dynamic adjustments of the PPC active power setpoint Pout at each PV plant. The FFT function continuously monitors the system, ensuring that the controller operates only when necessary and is deactivated once the oscillations are sufficiently mitigated. This optimized response prevents unnecessary interventions and highlights the adaptability of the control mechanism. The same sequence is applied during the second event, confirming the consistency of the POD-P controller's performance across different scenarios and grid conditions.

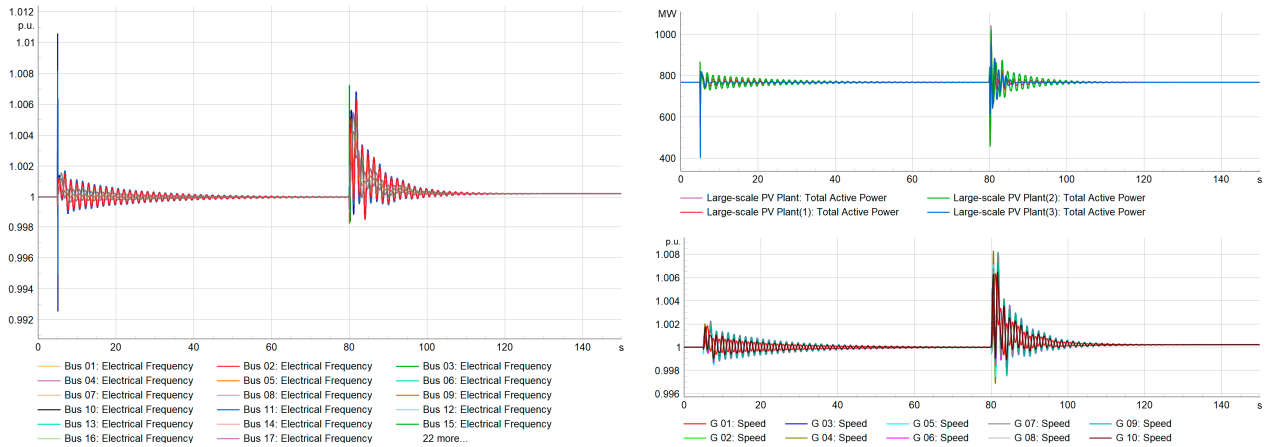

(**a**) (**b**)

Figure 7. Scenario 2. System response without the POD-P controller activated following the terminal short-circuit event (t = 5 s) and the line short-circuit event (t = 80 s): (**a**) frequency at all grid terminals [p.u.]; (**b**) frequency at PV terminals [p.u.] and speed of synchronous generators [p.u.].

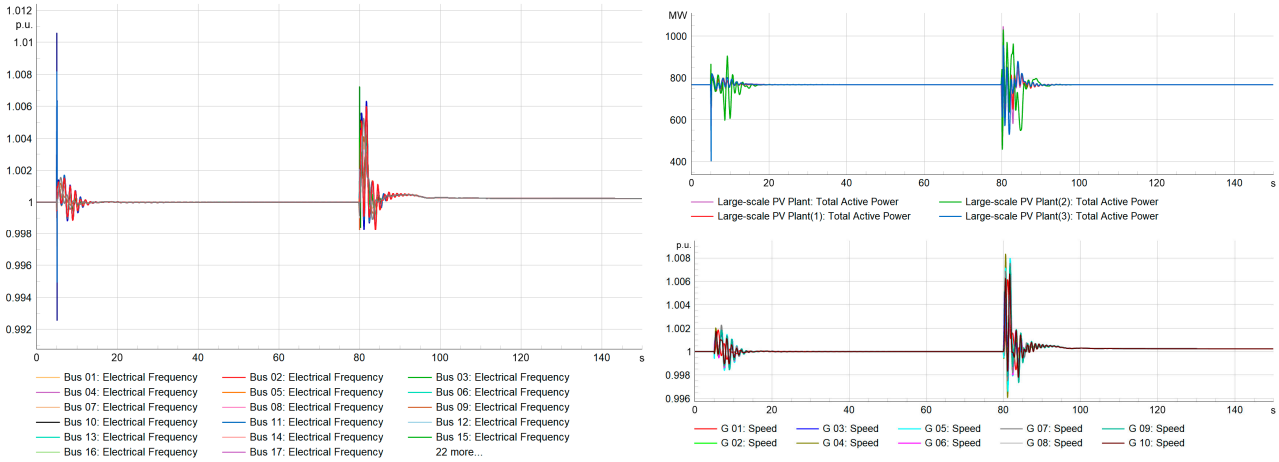

(**a**) (**b**)

Figure 8. Scenario 2. System response with the POD-P controller activated following the terminal short-circuit event (t = 5 s) and the line short-circuit event (t = 80 s): (**a**) frequency at all grid terminals [p.u.]; (**b**) frequency at PV terminals [p.u.] and speed of synchronous generators [p.u.].

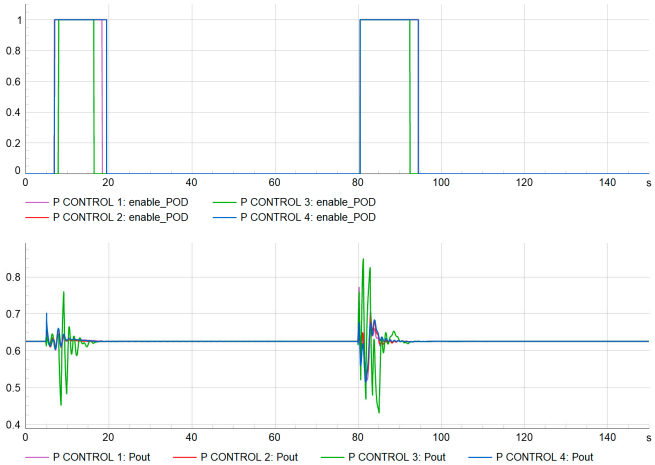

Figure 9. Scenario 2. POD-P activation signal *Enable_POD* and PPC active power setpoint *Pout* for each PV plant [p.u.].

8.3. Scenario 3

In Scenario 3, PV plants produce 80% of the total generation of the grid, operating at their full capacity (4912.64 MW), while synchronous generators supply only 20% (1245.9 MW, see Table 1). This scenario simulates extreme renewable integration, where the POD-P controller faces constraints due to the PV plants operating at their maximum capacity.

The first simulation, with the FFT detection function disabled, highlights the system's response under minimal synchronous generation conditions. The damping ratio of the electromechanical mode in this scenario is 1.12%, indicating lower system stability as the share of renewable increases. Figure 10a presents the frequency of the grid terminals. This response shows the smallest initial peak among the scenarios. This behavior, as previously noted in Scenario 2, is due to the reduced synchronous inertia, which lessens the system's ability to resist frequency changes after a disturbance. Moreover, the reduced damping ratio leads to the most prolonged oscillatory behavior of any scenario. Figure 10b focuses on the frequency at the PV plant terminals and the generator speeds.

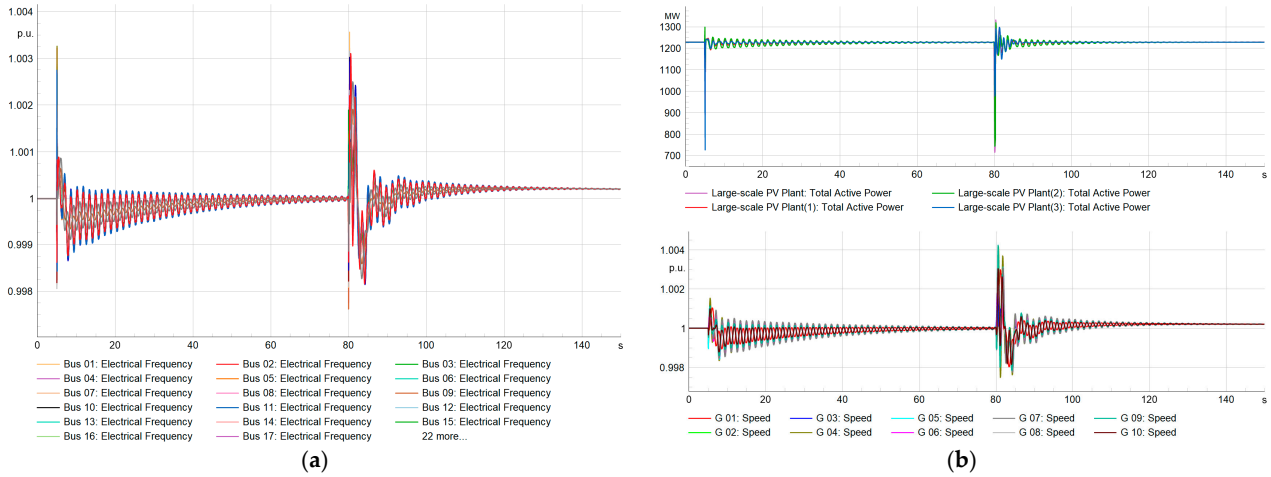

(**a**) (**b**)

Figure 10. Scenario 3. System response without the POD-P controller activated following the terminal short-circuit event (t = 5 s) and the line short-circuit event (t = 80 s): (**a**) frequency at all grid terminals [p.u.]; (**b**) frequency at PV terminals [p.u.] and speed of synchronous generators [p.u.].

When the FFT function is enabled, the POD-P controller damps inter-area oscillations by modulating the active power setpoint in the PPC. With the POD-P controller activated, the damping ratio improves to 9.16%, highlighting the controller's capability to enhance system stability even under high-renewable-penetration conditions. Figure 11a illustrates the significant reduction in frequency oscillations across all grid terminals, while Figure 11b confirms system stabilization at the PV terminals and synchronous generator speeds.

A limitation arises during the simulation, as highlighted in Figure 12: the PPC cannot further increase its active power setpoint because the PV plants are already operating at their maximum capacity (100%). This operational constraint leads to a slight but significant frequency drop (Figure 11a), which can critically affect system stability under conditions of high levels of renewable energy penetration. In systems dominated by inverter-based renewable generation, the absence of synchronous inertia further amplifies this vulnerability, increasing the grid's susceptibility to frequency deviations. If not properly managed, this issue can escalate into a frequency event, where reduced terminal frequencies threaten the grid's ability to operate within safe limits.

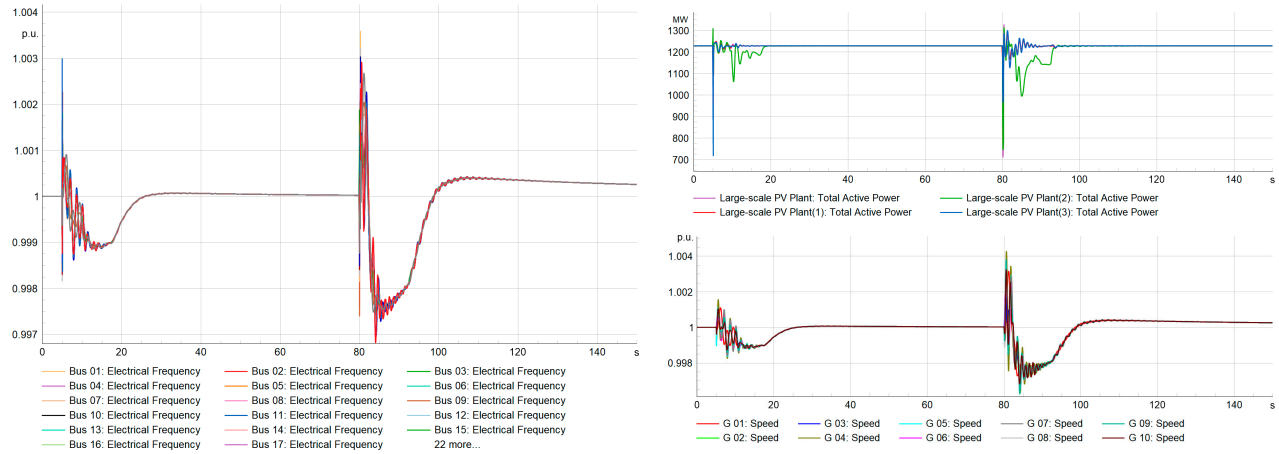

(**a**) (**b**)

Figure 11. Scenario 3. System response with the POD-P controller activated following the terminal short-circuit event (t = 5 s) and the line short-circuit event (t = 80 s): (**a**) frequency at all grid terminals [p.u.]; (**b**) frequency at PV terminals [p.u.] and speed of synchronous generators [p.u.].

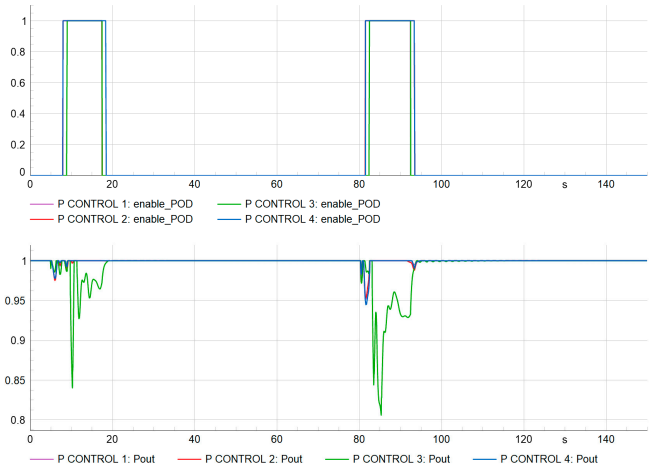

Figure 12. Scenario 3. POD-P activation signal *Enable_POD* and PPC active power setpoint Pout for each PV plant [p.u.].

To mitigate this limitation, simulations were repeated with the anti-windup filter of the PID controller activated. This filter effectively prevents excessive frequency deviations by constraining the controller's output, ensuring it does not drive the system beyond its physical limits. The advantages of this strategy are clearly demonstrated in Figures 13 and 14, where the initial frequency drop observed without the filter is successfully corrected. With the anti-windup filter activated, oscillations are rapidly damped and the system promptly returns to a steady state. This confirms the critical role of the filter in enhancing the robustness and reliability of the POD-P controller under saturation conditions.

To further quantify the performance of the POD-P controllers across these scenarios, Table 2 summarizes the electromechanical mode damping ratios for each scenario, with and without the POD-P controller activated.

Table 2. Damping ratio of each scenario, with and without the POD-P controller activated.

Damping Ratio [%]	Scenario 1	Scenario 2	Scenario 3
POD-P deactivated	3.19	1.76	1.12
POD-P activated	11.86	10.61	9.16

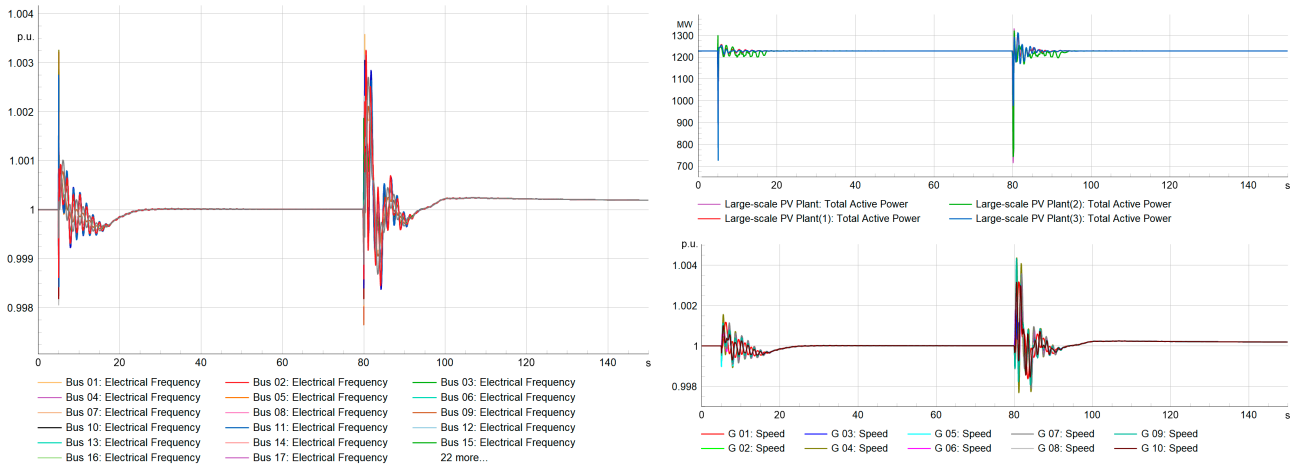

(**a**) (**b**)

Figure 13. Scenario 3 with anti-windup. System response with the POD-P controller activated following the terminal short-circuit event (t = 5 s) and the line short-circuit event (t = 80 s): (**a**) frequency at all grid terminals [p.u.]; (**b**) frequency at PV terminals [p.u.] and speed of synchronous generators [p.u.].

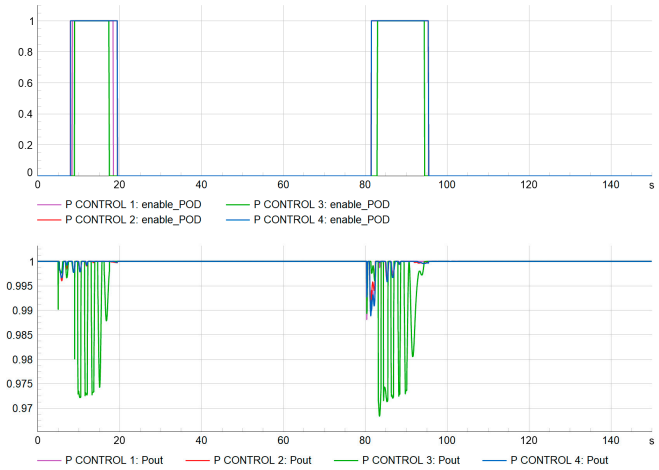

Figure 14. Scenario 3 with anti-windup. POD-P activation signal *Enable_POD* and PPC active power setpoint *Pout* for each PV plant [p.u.].

9. Discussion

The proposed FFT-enabled POD-P controller effectively detects and mitigates inter-area oscillations in scenarios with 20%, 50%, and 80% renewable penetration. The POD-P controller parameters are optimally tuned using the NBA to enhance its damping performance. Simulation results confirm that FFT-based detection reliably identifies oscillatory modes regardless of the share of renewable generation in the system. This capability enables the POD-P controller to activate upon the detection of oscillations, effectively damping the oscillations through dynamic adjustments to the PPCs' active power setpoint. Once the oscillations are mitigated, the POD-P controller deactivates, minimizing unnecessary interventions and ensuring operational efficiency. In all scenarios, the POD-P controller successfully reduces the oscillation amplitudes and stabilizes the system, achieving damping ratios above the stability threshold of 5%.

The system becomes less stable as renewable penetration increases, with reduced damping ratios observed in the electromechanical modes. This instability leads to prolonged oscillatory behavior, as seen in Scenarios 2 and 3. However, the initial frequency deviation following a disturbance is smaller in higher-renewable-penetration scenarios.

This behavior is attributed to diminished system inertia, which limits the system's ability to resist immediate changes in frequency following a disturbance, resulting in a smaller initial frequency deviation. The results highlight that while higher renewable integration increases the risk of sustained oscillations, the proposed POD-P controller mitigates these challenges, ensuring system stability.

Its ability to respond to successive disturbances further highlights the system's robustness. After resolving an initial disturbance, the FFT monitors system signals, reactivating the POD-P controller when subsequent events occur. This dynamic behavior ensures consistent stability, even under complex scenarios involving consecutive disturbances.

A notable improvement in the POD controller is the integrating of an anti-windup filter, addressing the limitations observed under high-renewable-energy scenarios. Saturation of the active power output restricts the controller's response, leading to a decrease in system frequency. The anti-windup filter ensures the correct operation of the controller under such conditions and maintains grid stability while preventing excessive frequency deviations.

The proposed methodology aligns with current regulatory frameworks, such as Commission Regulation (EU) 2016/631 and ACER Recommendation 03-2023 Annex 1, emphasizing the importance of renewable generators that include oscillation damping capabilities. Additionally, the Spanish draft Operation Procedure (PO) 12.2 explicitly requires Type D renewable plants to include POD controllers for inter-area oscillations from 0.1 Hz to 1.0 Hz. This demonstrates our methodology's practical applicability to meet regulatory standards.

These results demonstrate that the proposed approach is a reliable and flexible solution for managing inter-area oscillations, particularly in power systems with high renewable penetration. Future research will address the limitations encountered in high-renewable scenarios, such as photovoltaic saturation and renewable generation constraints, by exploring alternative solutions. Additionally, the methodology will be applied to more extensive grid systems to evaluate its performance and robustness under varying operational and topological complexities. The interaction between multiple controllers, such as PSS, POD-Q, and POD-P, will also be studied to assess their combined impact on grid stability. Moreover, hardware-in-the-loop (HiL) simulations will be explored to test a configuration wherein the PV plant is modeled in DSPF, while the PPC control and activation functions are deployed in an external PLC. This setup aims to enable certification and real-world validation of the PPC, ensuring its readiness for installation and operation as oscillation damping systems become increasingly critical.

10. Conclusions

This article presents a comprehensive and efficient methodology for detecting and mitigating inter-area oscillations in power systems with high levels of renewable energy penetration. By integrating FFT-based detection and an NBA-optimized POD-P controller within a unified simulation framework, the proposed approach offers a scalable and adaptable solution to the dynamic stability challenges modern grids face. This study's fundamental contribution lies in the seamless integration of oscillation detection, activation, and deactivation processes, demonstrating an ability to maintain grid stability under various operating conditions, including consecutive disturbances. The control system's robustness, enhanced by the inclusion of an anti-windup filter, effectively addresses constraints related to active power saturation, ensuring reliable operation even in scenarios featuring high levels of renewable energy production. The findings of this work provide a solid foundation for advancing oscillation-damping systems in grids dominated by renewable energy.

Author Contributions: Conceptualization, methodology, formal analysis, and investigation, M.B.-S.; software and validation, M.B.-S., M.M.-L. and P.F.-F.; resources and data curation, M.B.-S.; writing—original draft preparation, M.B.-S.; writing—review and editing, M.P.C., M.M.-L. and P.F.-F.; visualization, M.B.-S.; supervision, M.P.C.; project administration, M.B.-S.; funding acquisition, M.B.-S. All authors have read and agreed to the published version of the manuscript.

Funding: This research received no external funding.

Institutional Review Board Statement: Not applicable.

Informed Consent Statement: Not applicable.

Data Availability Statement: The original contributions presented in the study are included in the article, further inquiries can be directed to the corresponding author.

Acknowledgments: This work has been supported by the European Union's Horizon Europe Energy Research and Innovation program under the project eFORT (Grant Agreement no. 101075665). The content of this article reflects only the views of the authors. The European Commission is not responsible for any use that may be made of the information contained therein.

Conflicts of Interest: The authors declare no conflicts of interest.

References

1. Rogers, G. Power system structure and oscillations. *IEEE Comput. Appl. Power* **1999**, *12*, 14–21. [CrossRef]
2. Rogers, G.J. Control for stability in interconnected power systems. *IEEE Control. Syst. Mag.* **1989**, *9*, 19–22. [CrossRef]
3. Rogers, G. *Power System Oscillations*; Springer Nature: Dordrecht, The Netherlands, 2000. [CrossRef]
4. Kundur, P. *Power System Stability and Control*; McGraw-Hill, Palo Alto: Santa Clara, CA, USA, 1994.
5. Kosterev, D.N.; Taylor, C.W.; Mittelstadt, W.A. Model validation for the August 10, 1996 WSCC system outage. *IEEE Trans. Power Syst.* **1999**, *14*, 967–979. [CrossRef]
6. Chadwick, J.E. How a smarter grid could have prevented the 2003 U.S. cascading blackout. In Proceedings of the 2013 IEEE Power and Energy Conference at Illinois (PECI), Champaign, IL, USA, 22–23 February 2013; IEEE: Piscataway, NJ, USA, 2013; pp. 65–71. [CrossRef]
7. ENTSO-e. *Analysis of Ce Inter-Area Oscillations of 1st December 2016*; ENTSO-e: Brussels, Belgium, 2017; p. 13.
8. Dimitropoulos, D. Resonance Impact on Inter-Area Oscillations of the Nordic Power System. Master's Thesis, Universitat Politècnica de Catalunya, Barcelona, Spain, 2019; p. 85.
9. Seppanen, J.; Turunen, J.; Nikkila, A.-J.; Haarla, L. Resonance of Forcing Oscillations and Inter-Area Modes in the Nordic Power System. In Proceedings of the 2018 IEEE PES Innovative Smart Grid Technologies Conference Europe (ISGT-Europe), Sarajevo, Bosnia and Herzegovina, 21–25 October 2018; IEEE: Piscataway, NJ, USA, 2018; pp. 1–6. [CrossRef]
10. ENTSO-e. The Effects of System Extension on Inter-Area Oscillations. In *UCTE Annual Report 2002*; ENTSO-e: Brussels, Belgium, 2002.
11. Breulmann, H.; Grebe, E.; Losing, M.; Winter, W.; Witzmann, R.; Dupuis, P.; Houry, M.; Margotin, T.; Zerenyi, J.; Dudzik, J.; et al. Analysis and Damping of Inter-Area Oscillations in the UCTE/CENTREL Power System. *Eng. Environ. Sci. Phys.* **2000**.
12. Cai, D.; Ding, L.; Zhang, X.; Terzija, V. Wide area inter-area oscillation control system in a GB electric power system. *J. Eng.* **2019**, *2019*, 3294–3300. [CrossRef]
13. COMMISSION REGULATION (EU) 2016/631 of 14 April 201 Establishing a Network Code on Requirements for Grid Connection of Generators. Official Journal of the European Union. Available online: https://eur-lex.europa.eu/ (accessed on 24 April 2016).
14. ACER. *NC RfG DC Recommendation: Annex 1—Amended RfG Regulation*; ACER: New Taipei City, Taiwan, 2023.
15. Procedimiento de Operación (P.O.) 12.2 Instalaciones Conectadas a la red de Transporte Requisitos Mínimos de Diseño Equipamiento Funcionamiento y Seguridad y Pue.pdf. BOE Num. 51. Available online: https://www.cnmc.es/sites/default/files/editor_contenidos/Energia/Normativa_M_Electrico/P.O.%2012.2%20Instalaciones%20conectadas%20a%20la%20red%20de%20transporte%20-%20requisitos%20m%C3%ADnimos%20de%20dise%C3%B1o%20equipamiento%20funcionamiento%20y%20seguridad%20y%20puesta%20en%20servicio.pdf (accessed on 1 February 2025).
16. Red Eléctrica Española (REE), Redeia. *Guía Para la Implementación de Controles POD*; Red Eléctrica Española: Alcobendas, Spain, 2024; Volume 1, p. 31.
17. Restrepo, D.S.; Rios, M.A. Adaptive POD for STATCOM in a Power System with High Wind Power Penetration Level. In Proceedings of the 2019 IEEE Workshop on Power Electronics and Power Quality Applications (PEPQA), Manizales, Colombia, 30–31 May 2019; IEEE: Piscataway, NJ, USA, 2019; pp. 1–6. [CrossRef]

18. Singhavilai, N.J.Y.T. Observation of applying POD function to renewable energy source. In Proceedings of the 2016 International Conference on Cogeneration, Small Power Plants and District Energy (ICUE), Bangkok, Thailand, 14–16 September 2016; IEEE: Piscataway, NJ, USA, 2016; pp. 1–5. [CrossRef]
19. Mithulananthan, N.; Canizares, C.A.; Reeve, J.; Rogers, G.J. Comparison of PSS, SVC, and STATCOM controllers for damping power system oscillations. *IEEE Trans. Power Syst.* **2003**, *18*, 786–792. [CrossRef]
20. Li, M.; Xiong, L.; Chai, H.; Xiu, L.; Hao, J. Mechanism of PV Generation System Damping Electromechanical Oscillations. *IEEE Access* **2020**, *8*, 135853–135865. [CrossRef]
21. Babu, A.S.; Subadhra, P.R. Power Oscillation Damping By Utilizing PV-STATCOM. In Proceedings of the 2022 IEEE Delhi Section Conference (DELCON), New Delhi, India, 11–13 February 2022; IEEE: Piscataway, NJ, USA, 2022; pp. 1–6. [CrossRef]
22. Alalwani, S.; Isik, S.; Bhattacharya, S. Inter-area Oscillation Damping Controller for DFIG based Wind Power Plants. In Proceedings of the 2022 IEEE Energy Conversion Congress and Exposition (ECCE), Detroit, MI, USA, 9–13 October 2022; IEEE: Piscataway, NJ, USA, 2022; pp. 1–6. [CrossRef]
23. Mansour, W.; Mandour, M.; El-Shimy, M.; Bendary, F. Impact of Wind Power on Power System Stability and Oscillation Damping Controller Design. In Proceedings of the Industry Academia Collaboration (IAC) Conference, New Delhi, India, 13–14 February 2025.
24. Arvani, A.; Rao, V.S. Power oscillation damping controller for the power system with high wind power penetration level. In Proceedings of the 2014 North American Power Symposium (NAPS), Pullman, WA, USA, 7–9 September 2014; IEEE: Piscataway, NJ, USA, 2014; pp. 1–6. [CrossRef]
25. Pillai, A.G.; Thomas, P.C.; Sreerenjini, K.; Baby, S.; Joseph, T.; Srecdharan, S. Transient stability analysis of wind integrated power systems with storage using central area controller. In Proceedings of the 2013 Annual International Conference on Emerging Research Areas and 2013 International Conference on Microelectronics, Communications and Renewable Energy, Kanjirapally, India, 4–6 June 2013; IEEE: Piscataway, NJ, USA, 2013; pp. 1–5. [CrossRef]
26. Ali, H.R.; Hoonchareon, N. Real-time monitoring of inter-area power oscillation using Phasor Measurement Unit. In Proceedings of the 2013 10th International Conference on Electrical Engineering/Electronics, Computer, Telecommunications and Information Technology, Krabi, Thailand, 15–17 May 2013; IEEE: Piscataway, NJ, USA, 2013; pp. 1–6. [CrossRef]
27. Erlich, I.; Hashmani, A.; Shewarega, F. Selective damping of inter area oscillations using phasor measurement unit (PMU) signals. In Proceedings of the 2011 IEEE Trondheim PowerTech, Trondheim, Norway, 19–23 June 2011; IEEE: Piscataway, NJ, USA, 2011; pp. 1–6. [CrossRef]
28. Visakhan, R.; Rahul, R.; Hridya, K.R.; Kurian, A.A. Analysis of power oscillation damping capability of STATCOM-POD and optimal placement of PMUs in IEEE-14 bus system. In Proceedings of the 2015 International Conference on Power, Instrumentation, Control and Computing (PICC), Thrissur, India, 9–11 December 2015; IEEE: Piscataway, NJ, USA, 2015; pp. 1–7. [CrossRef]
29. Trudnowski, D.; Kosterev, D.; Undrill, J. PDCI damping control analysis for the western North American power system. In Proceedings of the 2013 IEEE Power & Energy Society General Meeting, Vancouver, BC, Canada, 21–25 July 2013; IEEE: Piscataway, NJ, USA, 2013; pp. 1–5. [CrossRef]
30. Chowdhary, G.; Srinivasan, S.; Johnson, E. Frequency Domain Method for Real-Time Detection of Oscillations. In Proceedings of the AIAA Infotech@Aerospace 2010, Atlanta, GA, USA, 20–22 April 2010; American Institute of Aeronautics and Astronautics: Reston, VA, USA, 2010. [CrossRef]
31. Khayyatzadeh, M.; Kazemzadeh, R. Sub-synchronous resonance damping using high penetration PV plant. *Mech. Syst. Signal Process.* **2017**, *84*, 431–444. [CrossRef]
32. Xiong, W.; Wang, L.; Wu, R.; Qi, Y.; Liu, H.; Bi, T. Decision Tree Based Subsynchronous Oscillation Detection and Alarm Method Using Phasor Measurement Units. In Proceedings of the 2020 IEEE Sustainable Power and Energy Conference (iSPEC), Chengdu, China, 23–25 November 2020; IEEE: Piscataway, NJ, USA, 2020; pp. 2448–2453. [CrossRef]
33. Peng, J.C.-H.; Nair, N.-K.C. Effects of Sampling in Monitoring Power System Oscillations Using On-line Prony Analysis. In Proceedings of the 2008 Australasian Universities Power Engineering Conference, Sydney, NSW, Australia, 14–17 December 2008.
34. Foyen, S.; Kvammen, M.-E.; Fosso, O.B. Prony's method as a tool for power system identification in Smart Grids. In Proceedings of the 2018 International Symposium on Power Electronics, Electrical Drives, Automation and Motion (SPEEDAM), Amalfi, Italy, 20–22 June 2018; IEEE: Piscataway, NJ, USA, 2018; pp. 562–569. [CrossRef]
35. Terzija, V.; Cai, D.; Fitch, J. Monitoring of inter-area oscillations in power systems with renewable energy resources using Prony method. In Proceedings of the CIRED 2009-20th International Conference and Exhibition on Electricity Distribution-Part 1, Prague, Czech Republic, 8–11 June 2009; p. 746. [CrossRef]
36. Katariya, K.; Pradhan, A.K.; Bajpai, P. Matrix Pencil Method Based Oscillation Monitoring—A Case Study in 240-Bus WECC Test System. In Proceedings of the 2022 International Conference on Intelligent Controller and Computing for Smart Power (ICICCSP), Hyderabad, India, 21–23 July 2022; IEEE: Piscataway, NJ, USA, 2022; pp. 1–6. [CrossRef]

37. Chitturi, S.; Chakrabarti, S.; Singh, S.N. Comparing performance of Prony analysis and matrix pencil method for monitoring power system oscillations. In Proceedings of the 2014 IEEE Innovative Smart Grid Technologies—Asia (ISGT ASIA), Kuala Lumpur, Malaysia, 20–23 May 2014; IEEE: Piscataway, NJ, USA, 2014; pp. 447–452. [CrossRef]
38. Mahapatra, S.; Jha, A. PSS & TCSC coordinated design using particle swarm optimization for power system stability analysis. In Proceedings of the 2012 2nd International Conference on Power, Control and Embedded Systems, Allahabad, India, 17–19 December 2012; IEEE: Piscataway, NJ, USA, 2012. [CrossRef]
39. Edrah, M.; Zhao, X.; Hung, W.; Qi, P.; Marshall, B.; Karcanias, A.; Baloch, S. Effects of POD Control on a DFIG Wind Turbine Structural System. *IEEE Trans. Energy Convers.* **2020**, *35*, 765–774. [CrossRef]
40. Miotto, E.L.; Araujo, P.B.D.; Takahashi, L.M.A.; Fortes, E.D.V. Tuning of the parameters of damping controllers for power electrical systems using Bioinspired Algorithms. In Proceedings of the 2018 13th IEEE International Conference on Industry Applications, São Paulo, Brazil, 12–14 November 2018; IEEE: Piscataway, NJ, USA, 2018. [CrossRef]
41. Islam, N.N.; Hannan, M.A.; Shareef, H.; Mohamed, A. Power system stabilizer design using BAT optimization algorithm in multimachine power system. In Proceedings of the 2013 IEEE Student Conference on Research and Developement, Putrajaya, Malaysia, 16–17 December 2013; IEEE: Piscataway, NJ, USA, 2013; pp. 540–544. [CrossRef]
42. Miotto, E.L.; Covacic, M.R. Study of Stability Dynamic in a Multimachine Power System Using Robust Controllers PSS and POD. In Proceedings of the 2011 Asia-Pacific Power and Energy Engineering Conference, Wuhan, China, 25–28 March 2011; IEEE: Piscataway, NJ, USA, 2011; pp. 1–5. [CrossRef]
43. Abd-Elazim, S.; Ali, E. Coordinated design of PSSs and SVC via bacteria foraging optimization algorithm in a multimachine power system. *Int. J. Electr. Power Energy Syst.* **2012**, *41*, 44–53. [CrossRef]
44. PowerFactory DIgSILENT. [En Línea]. Available online: https://www.digsilent.de/en/powerfactory.html (accessed on 15 January 2025).
45. Bernal-Sancho, M.; Comech, M.P.; Galan-Hernandez, N. Bibliographic Review on Power Oscillation Detection Methods. In Proceedings of the NEIS 2023: Conference on Sustainable Energy Supply and Energy Storage Systems, Hamburg, Germany, 4 September 2023.
46. Bernal-Sancho, M.; Comech, M.P.; Galán-Hernández, N. Damping control in renewable-integrated power systems: A comparative analysis of PSS, POD-P, and POD-Q strategies. *Int. J. Electr. Power Energy Syst.* **2024**, *162*, 110308. [CrossRef]
47. Bernal-Sancho, M.; Comech, M.P.; Galan-Hernandez, N. Coordinated tuning of STATCOM-POD controllers using PSO and NBA: A case study in DIgSILENT PowerFactory. In Proceedings of the ICSC-CITIES 2024, VII Ibero-American Congress of Smart Cities, San Carlos, Costa Rica, 12 November 2024.
48. Yang, X.S. A new metaheuristic bat-inspired algorithm. In *Nature Inspired Cooperative Strategies for Optimization*; Studies in Computational Intelligence; Springer: Berlin/Heidelberg, Germany, 2010; Volume 284, pp. 65–74.
49. Wang, Y.; Wang, P.; Zhang, J.; Cui, Z.; Cai, X.; Zhang, W.; Chen, J. A Novel Bat Algorithm with Multiple Strategies Coupling for Numerical Optimization. *Mathematics* **2019**, *7*, 135. [CrossRef]
50. Fortes, E.V.; Martins LF, B.; Miotto, E.L.; Araujo, P.B.; Macedo, L.H.; Romero, R. Artificial Bee Colony Algorithm Based Approach for Power System Oscillation Damping with PSS and STATCOM. *Int. J. Res. Stud. Electr. Electron. Eng.* **2019**, *5*, 121–136. [CrossRef]
51. Ministerio de Industria, Turismo y Comercio. Procedimiento de Operación 13.1. Criterios de Desarrollo de la Red de Transporte. BOE Núm. 85. Available online: https://www.boe.es/boe/dias/2005/04/09/pdfs/A12351-12358.pdf (accessed on 9 April 2005).
52. DIgSILENT PowerFactory. IEEE 39 Bus New Engalnd System. Available online: https://www.scribd.com/document/341527272/39-Bus-New-England-System (accessed on 1 February 2025).
53. Pai, M.A. *Energy Function Analysis for Power System Stability*; Springer: Boston, MA, USA, 1989. [CrossRef]
54. Kamwa, I.; Grondin, R.; Trudel, G. IEEE PSS2B Versus PSS4B: The Limits of Performance of Modern Power System Stabilizers. *IEEE Trans. Power Syst.* **2005**, *20*, 903–915. [CrossRef]
55. Ministerio Para la Transición Ecológica y el Reto Demográfico (MITECO). Plan Nacional Integrado de Energía y Clima (PNIEC). Actualización 2023–2030, Madrid September 2024. Available online: https://www.miteco.gob.es/content/dam/miteco/es/energia/files-1/pniec-2023-2030/PNIEC_2024_240924.pdf (accessed on 1 February 2025).